Materials Science Forum Vol. 590 (2008) pp 233-248
online at http://www.scientific.net

Impact of Point Defects on the Luminescence Properties of (Al,Ga)N

Shigefusa F. Chichibu[1,2,a], Akira Uedono[3,b], Takeyoshi Onuma[1,2], Steven P. DenBaars[2,4], Umesh K. Mishra[4], James S. Speck[2,4], and Shuji Nakamura[2,4]

[1]Center for Advanced Nitride Technology, Institute of Multidisciplinary Research for Advanced Materials, Tohoku University, 2-1-1 Katahira, Aoba, Sendai 980-8577, Japan

[2]Nakamura Inhomogeneous Crystal Project, ERATO, Japan Science and Technology Agency, Kawaguchi 332-0012, Japan

[3]Institute of Applied Physics, University of Tsukuba, Tsukuba 305-8573, Japan

[4]Materials and ECE Departments, University of California, Santa Barbara, California 93016, USA

[a]chichibulab@yahoo.co.jp, [b]uedono@sakura.cc.tsukuba.ac.jp

Keywords: GaN, AlN, AlGaN, point defect, vacancy, nonradiative recombination, emission efficiency, luminescence.

Abstract. Threading dislocations (TDs) in (Al,In,Ga)N semiconductors are known to affect the luminescence efficiency of near-band-edge (NBE) emissions in bulk films and quantum structures. However, the principal role of *point defects* such as vacancies on the luminescent properties has not been fully understood. In this article, impacts of point defects on the luminescence quantum efficiency of NBE emissions and on the intensity of deep emission bands will be described, based on the results of steady-state and time-resolved photoluminescence (TRPL) and positron annihilation measurements. The room temperature nonradiative lifetime (τ_{NR}) of the NBE excitonic photoluminescence (PL) peak in polar (0001) and (000-1) , nonpolar (11-20) and (10-10), and zincblende (001) GaN layers prepared by various growth techniques was shown to increase with the decrease in concentration or size of Ga vacancies (V_{Ga}) and with the decrease in gross concentration of point defects including complexes, leading to an increase in the NBE PL intensity. As the edge TD density decreased, the concentration or size of V_{Ga} tended to decrease and τ_{NR} tended to increase. However, there existed remarkable exceptions. The results indicate that the nonradiative recombination process is governed not by single point defects, but by certain defects introduced with the incorporation of V_{Ga}, such as V_{Ga}-defect complexes. Similar relations were found in $Al_xGa_{1-x}N$ alloy films grown by metalorganic vapor phase epitaxy: *i. e.* τ_{NR} at room temperature increased with the decrease in the concentration of cation vacancies (V_{III}) and with the decrease in gross concentration of point defects. In addition to nonradiative processes, the V_{III} concentration was found to correlate with the intensity ratio of characteristic deep emission band to the NBE emission (I_{deep}/I_{NBE}). For example, I_{deep}/I_{NBE} at low temperature for the deep emission bands at 4.6, 3.8, and 3.1 eV of AlN epilayers grown by NH_3-source molecular beam epitaxy had a linear correlation with the concentration or size of Al vacancies (V_{Al}). Since the relative intensities of 3.1 eV and 3.8 eV bands increased remarkably with lowering the supply ratio of NH_3 to Al (V/III ratio) and growth temperature (T_g), they were assigned to originate from V_{Al}-O as well as V_{Al}-shallow donor complexes. The V_{Al} concentration could be decreased by adjusting the V/III ratio and T_g. In the case of $Al_xGa_{1-x}N$ alloys, the concentration or size of V_{III} and I_{deep}/I_{NBE} at 300 K increased simultaneously with the increase in x up to approximately 0.7. Similar to the case for GaN and AlN, the deep emission band was assigned as being due to the emission involving V_{III}-O complexes.

Introduction

GaN and related group-III nitride alloys [1,2] are providing enormous practical benefits in producing blue and green light emitting diodes (LEDs) for multicolour displays and traffic signals, white LEDs

for solid-state lighting, and 400 nm laser diodes (LDs) for high density optical storage. The bandgap energies of these materials are 0.65 eV for InN, 3.43 eV for GaN, and 6.04 eV for AlN at room temperature. Therefore, (Al,In,Ga)N alloys are promising materials for realization of light emitters and detectors operating in the infrared to deep ultraviolet (UV) wavelength regions. However, due to the lack of lattice-matched or homoepitaxial substrates, (Al,In,Ga)N heterostructure LEDs have largely been fabricated on the (0001) *c*-plane of Al_2O_3 substrates. Because of the lattice mismatch between the base GaN layer and the Al_2O_3 substrate ($\Delta a/a \cong 16$ %), the GaN films usually contain a high density of structural defects such as threading dislocations (TDs) and stacking faults (SFs). For example, the TD density (TDD) in LED structures has been revealed to be as high as 10^9-10^{10} cm^{-2} [3], which is six orders of magnitude higher than that in conventional AlGaAs (red) or AlInGaP (amber) LED films.

An important but frequently overlooked fact is that all commercially available high efficiency blue, green, and white light-emitting diodes (LEDs) and purple (400 nm) laser diodes (LDs) [1,2] use InGaN quantum wells (QWs), not GaN or AlGaN alloys, since excitons localized [4] at In-rich quantum nanoclusters [4-7] or at -In-N- bonds [8-12] in InGaN exhibit high quantum efficiency (η) even though the TDD is as high [3] as 10^9 cm^{-2}. We note that there exist plenty of other explanations on this fact [13-25] and the matter is still under debate [11,12].

Apart from In-containing materials, high quality GaN and AlGaN alloys of reduced nonradiative recombination center (NRC) density are indispensable to realize UV LEDs and LDs. In addition to extended defects such as TDs and SFs, there naturally exist microscopic ones such as point defects [27-34], complexes, and impurities (O, C, and Si) in (Al,In,Ga)N crystals. Although it is not yet clear whether TDs themselves act as NRCs, TDs are often assigned to the origin of NRCs [26]. Indeed, the NRC concentration in GaN was shown to have a fairly good correlation with the TDD [11,12,35]. However, because GaN of low TDD often exhibits low internal quantum efficiency (η_{int}) [11] up to a few percent, the relation between the nonradiative luminescence lifetime (τ_{NR}) and the point defect density must be compared. Here we note that η_{int} at 300 K is approximated as the spectrally integrated photoluminescence (PL) intensity at 300 K divided by that at 8 K [I_{PL}(300K) / I_{PL}(8K)] [36] in the weak excitation regime (a few W/cm^2) throughout this article, where the relaxation efficiency toward the radiative near-band-edge (NBE) states is assumed to be nearly independent on temperature.

In this article, the impact of point defects on η_{int} of the NBE emissions and on the intensity ratio of characteristic deep emission bands to the NBE emission (I_{deep}/I_{NBE}) of GaN, AlN, and AlGaN alloys will be reviewed, based on the results of steady-state and time-resolved photoluminescence (TRPL) and positron annihilation measurements [37,38]. In-containing alloys are excluded, because they exhibit characteristic emission properties originating from -In-N- bonds [11,12].

Experimental Procedures and General Results

Samples. To elucidate the atomistic origin of NRCs, GaN films and crystals having a variety of TDD were prepared to study the relation between τ_{NR} and point defect density [35]. They were (i) 80-μm-thick free-standing undoped (0001) GaN grown by metalorganic vapor phase epitaxy (MOVPE) using lateral epitaxial overgrowth (LEO) technique on a (0001) Al_2O_3 substrate followed by polishing away the substrate (abbreviated by 'bulk GaN') [39], (ii) 1~5-μm-thick undoped (0001) Ga-polar GaN grown by MOVPE on (0001) Al_2O_3 ['uid +*c*(1)' and 'uid +*c*(5)'] [40,41], (iii) 0.7-μm-thick unintentionally O-doped (5×10^{18} cm^{-3}) (000-1) N-polar GaN grown by MOVPE on (0001) Al_2O_3 ['uid -*c*'] [41], (iv) Si-doped 2-μm-thick (0001) GaN on (0001) Al_2O_3 [31,35] [Si-dope(1.6E18), Si-dope(1.9E18), and Si-dope(2.2E18), with doping concentrations in parentheses], (v) 1-μm-thick unintentionally O-doped ($\cong10^{18}$ cm^{-3}) cubic (001) GaN grown by MOVPE on (001) GaAs with or without AlGaN/GaN superlattice buffer layer ['ZB(no SL)' and 'ZB(SL)'] [42], (vi) 1-μm-thick unintentionally O-doped (001) GaN grown by N_2 rf-plasma-assisted molecular-beam epitaxy (MBE) on (001) 3C-SiC with AlN/GaN multiple buffer layer ['ZB(MBE)']

[35] , (vii) 15~16-μm-thick undoped (11-20) GaN grown by halide vapor phase epitaxy (HVPE) on (10-12) Al_2O_3 with or without LEO-GaN base ['*a*-GaN(LEO)' and '*a*-GaN'] [43], and (viii) free-standing unintentionally O-doped (>10^{18} cm^{-3}) (10-10) GaN grown by HVPE on $LiAlO_2$ followed by delamination ['*m*-GaN(FS)'] [35]. The TDD of these samples was varied between 10^5 and 10^{10} cm^{-2} [35].

Approximately 0.7~1-μm-thick AlN epilayers were grown by ammonia source molecular-beam epitaxy (NH_3-MBE) [44] on a 2-μm-thick GaN epitaxial template layer prepared by MOVPE on a (0001) Al_2O_3 substrate. Filtered 99.999%-pure NH_3 and 99.9999%-pure metallic Al were used as the sources. The growth was initiated with a deposition of an AlN interlayer (IL-AlN) [45], which was 10~20-nm-thick AlN deposited at 270°C followed by an annealing at 900°C in NH_3 ambient. Then, AlN epilayers were grown at 890 and 970 °C. The supply ratio of NH_3 to Al (V/III ratio) was varied between 60 and 433 by varying the beam equivalent pressure (BEP) of NH_3 (1.8×10^{-3} to 1.3×10^{-2} Pa) with a fixed BEP of Al (2.2×10^{-5} Pa). The IL-AlN had two major roles. One is to prevent the GaN template from decomposing during the heating prior to the growth. Another role is to coordinate the in-plane lattice mismatch between AlN and GaN (3.3%) at an early stage of the growth. As a result, the present AlN epilayers did not exhibit macroscopic or microscopic cracks, and the epilayers had little strain. No noticeable change was found in the surface atomic force microscopy images of all the samples. However, the full-width at half maximum (FWHM) value of the asymmetric (10-12) AlN diffraction peak of the x-ray rocking curve (XRC) ($\Delta\omega_{(10\text{-}12)}$) was influenced by the V/III ratio. For example, $\Delta\omega_{(10\text{-}12)}$ took the smallest value for the sample grown with V/III=150, and the value significantly increased for V/III=60. The TDD having edge components was estimated from the $\Delta\omega_{(10\text{-}12)}$ values [46] to be in the range between 10^{10} and 10^{11} cm^{-2}.

Approximately 1-μm-thick nearly strain-free (0001) $Al_xGa_{1-x}N$ films [47] were grown by MOVPE on an $Al_{0.63}Ga_{0.37}N$ low-temperature nucleation layer (NL) on (0001) Al_2O_3 substrate. The TDD was approximately 10^9-10^{10} cm^{-2}.

Steady-State and Time-Resolved Photoluminescence Measurements. Steady-state NBE photoluminescence (PL) of the samples having the bandgap energy lower than 3.6 eV was excited by the 325.0 nm line of a cw He-Cd laser. For the higher bandgap films, PL was excited by an approximately 100 fs pulse of a frequency doubled or tripled mode-locked Al_2O_3:Ti laser (Spectra Physics, Tsunami 3940 and GWU-23FS), of which the wavelength λ was chosen between 240 and 380 nm to selectively excite each film of interest. The repetition rate and excitation density were 80 MHz and approximately 200 nJ/cm^2 per pulse, respectively. In both cases, phase-sensitive detection was carried out using a mechanical chopper driven at a few hundred Hz to acquire the PL signal.

TRPL signal was collected using a standard streak-camera acquisition technique (Hamamatsu, C4334-01). The excitation source was the same Al_2O_3:Ti laser. Representative normalized TRPL signals for the NBE emission peak in GaN films and an $Al_{0.35}Ga_{0.65}N$ alloy film at 293K are summarized in Fig. 1. Because the samples exhibited different decay rates

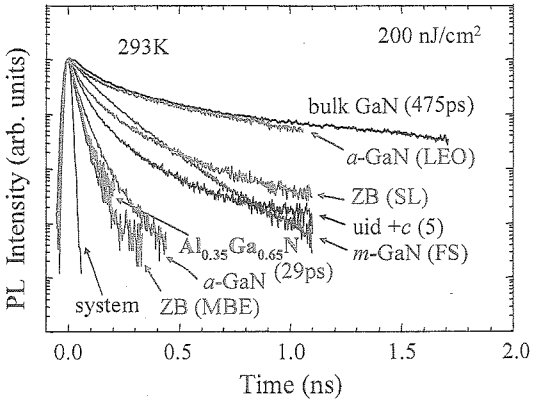

Fig. 1. Representative normalized TRPL signals of the variety of GaN samples and $Al_{0.35}Ga_{0.65}N$ alloy film at 293 K. The black line denoted by 'system' represents the system response (after Refs. [11,12,35, 47]).

with non-identical decay shapes, which can be fitted by a single- or a double-exponential function, the effective PL lifetime ($\tau_{PL,eff}$) was introduced to compare the recombination processes taking place in different samples. The value of $\tau_{PL,eff}$ is defined [11] as the time after excitation when

$$\int_0^{\tau_{PL,eff}} I(t)dt \Big/ \int_0^{t_{lim}} I(t)dt \tag{1}$$

becomes 1-1/e, where $I(t)$ is the intensity at time t and t_{lim} is defined as the time when $I(t_{lim})$ becomes $0.01I(0)$. Values of $\tau_{PL,eff}$ for bulk GaN and $Al_{0.35}Ga_{0.65}N$ alloy samples are displayed in Fig. 1. The effective radiative lifetime ($\tau_{R,eff}$) and effective nonradiative lifetime ($\tau_{NR,eff}$) at room temperature were deduced from the experimental values of $\tau_{PL,eff}$ and η_{int} using the relations

$$\frac{1}{\tau_{PL,eff}} = \frac{1}{\tau_{R,eff}} + \frac{1}{\tau_{NR,eff}} \tag{2}$$

and

$$\eta_{int} = \frac{1}{1 + \tau_{R,eff} \Big/ \tau_{NR,eff}}. \tag{3}$$

Monoenergetic Positron Annihilation Measurements. Positron annihilation is a unique method for the direct detection of point defects in a condensed matter [28,31,37,38]. When a positron is implanted into condensed matter, it annihilates with a surrounding electron and emits two 511 keV γ rays according to $E=mc^2$, where E is energy, m the mass, and c the speed of the light. The γ rays are broadened due to the momentum component of the annihilating positron-electron pair. Since the momentum distribution of electrons around negatively-charged or neutral vacancy defects is smaller in defect-free regions, the defects can be detected by measuring the Doppler broadening spectra of the annihilation γ rays. The resulting change in the γ ray spectra is characterized by the S parameter [28,31,37,38], which represents the fraction of annihilating positron-electron pairs of small momentum distribution. Since cation vacancies (V_{III}) and their complexes have negative charges and form acceptor-type defects in n-type (Al,In,Ga)N [27,32,34], they are the most probable [28,31] candidates of positron trapping centers. Therefore, S increases with the increase in concentration or size of V_{III} and V_{III}-complexes. Schematic illustrations of a positron in defect-free region and a positron trapped by a negatively charged Ga vacancie (V_{Ga}^-) in GaN are shown in Figs. 2(a) and 2(b), respectively.

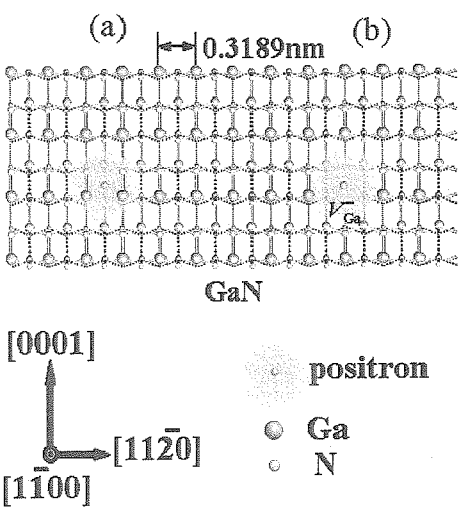

Fig. 2. Schematic representations of a positron (a) freely diffusing in defect-free regions and (b) trapped by negatively charged V_{Ga} in GaN. For simplicity, four atomic planes parallel to the m-plane {10-10} are drawn (after Refs. [11,12]).

For multilayer structures, the characteristic S value and positron diffusion length (L_+) in each layer can be determined by using a monoenergetic

positron beam [38], by which the mean implantation depth of positrons can be adjusted. The analysis [28,31,38,48] involves solving the diffusion equation of positrons using the initial implantation profile as a function of positron acceleration energy E, as described below. Here, L_+ can be used as a measure of the gross concentration of positron trapping centers and scattering centers, because both of them decrease L_+ [11,12,31,35]. The trapping centers are V_{III} and V_{III}-complexes and the scattering centers are positively-charged and neutral point defects such as [34] N vacancies V_N, group-III interstitials III_i, and complexes. We note that this argument is applicable for condensed matter that does not contain particular (exotic) positron trapping centers.

A monoenergetic positron beam line [31] was used to measure the Doppler broadening spectra of annihilation radiation as a function of E. For each value of E, a γ-ray spectrum with 5×10^5 total counts was measured. The S parameter was defined as the number of annihilation events for the energy range 511±0.76 keV over the total counts. The S-E relation was analyzed using the algorithm named *VEPFIT*, a computer program developed by van Veen *et al.*[48] The one dimensional diffusion model of positrons is expressed by [38]

$$D_+ \frac{d^2}{dz^2} n(z) - \kappa_{eff}(z) n(z) + P(z,E) = 0, \tag{4}$$

where D_+ is the diffusion coefficient of positrons, $n(z)$ the probability density of positrons at a distance z from the surface, $\kappa_{eff}(z)$ the effective escape rate of positrons from the diffusion process, and $P(z,E)$ the implantation profile of positrons. The diffusion length of positrons $L_+(z)$ is given by

$$L_+(z) = \sqrt{D_+ / \kappa_{eff}(z)}. \tag{5}$$

In the fitting procedure, the region probed by positrons was divided into two or three blocks, namely the (Al,Ga)N layer, the GaN template, and the substrate if they were present. Under these conditions, *VEPFIT* was used to determine the fraction of positrons annihilated in each block and the corresponding S parameter. The S-E curve was fitted to the following equation:

$$S(E) = S_s F_s(E) + \sum S_i F_i(E), \tag{6}$$

where $F_s(E)$ is the fraction of positrons annihilated at the surface and $F_i(E)$ is the fraction of positrons annihilated in the ith block [$F_s(E)+\Sigma F_i(E) = 1$], and S_s and S_i are the S parameters of the surface and in the ith block, respectively. The analytical procedures used in this study were similar to those described in Ref. [31].

S-E curves for free-standing bulk c-plane GaN, 1-μm-thick nearly strain-free c-plane $Al_{0.35}Ga_{0.65}N$ / Al_2O_3, and several GaN samples are shown in Fig. 3. The mean implantation depth of positrons calculated for GaN is given on the upper horizontal axis. For bulk GaN, S approached a constant value at high E (>10 keV), which indicates that in this energy

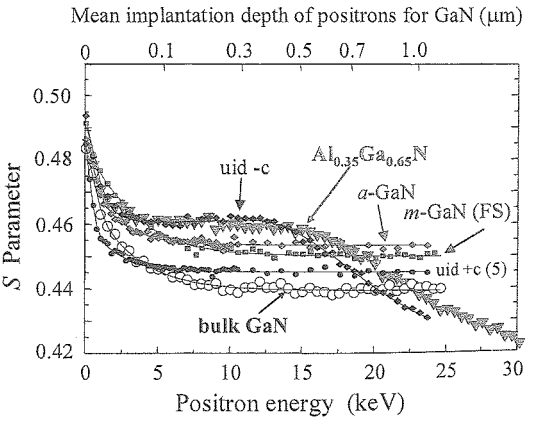

Fig. 3. Doppler broadening S parameter at room temperature for the representative GaN and $Al_{0.35}Ga_{0.65}N$ samples as a function of positron acceleration energy E (S-E relation).

range, almost all positrons annihilate in the bulk region without diffusing back to the surface. The increase in S at low E ($\cong$0 keV) is due to the annihilation of positrons and positronium atoms at the surface. The thin solid curve is the fitting result, and L_+ and S were determined to be 51±2 nm and 0.4401±0.0001, respectively [31]. This S value was defined as a characteristic S value for the positron-electron pairs annihilating in defect-free regions (S_{free}) in bulk GaN [see Fig. 2(a)]. Similarly, S and L_+ values particular to other GaN and AlGaN films were determined: S was obtained for E>15 keV for a-GaN and m-GaN (FS) and 5 keV<E<10 keV for uid -c and $Al_{0.35}Ga_{0.65}N$. Note that the decrease in S for high E (>15 keV) in uid -c and AlGaN is due to the annihilation of positrons in the Al_2O_3 substrate, which has a different (low) S_{free} value.

Results and Discussion

GaN study. Values of $\tau_{PL,eff}$ at 293 K of the GaN samples are plotted in Fig. 4(a) as a function of edge component TDD. We note that the samples represented by closed symbols in Figs. 4-6 were unintentionally doped with O, as evidenced by secondary-ion mass spectrometry (SIMS). Although the experimental data are not shown, the steady-state PL intensity naturally increased with increasing $\tau_{PL,eff}$ according to the relation given by Eq. 3, where $\tau_{R,eff}$ is constant for three-dimensional (3D) GaN. The value of $\tau_{PL,eff}$ tended to increase with decreasing TDD. However, there were remarkable exceptions such as m-GaN(FS) and uid -c; correlation between $\tau_{PL,eff}$ and TDD was incomplete. Hence, microscopic point defects in the materials were investigated by the positron annihilation technique.

Values of S and L_+ of GaN samples obtained from the monoenergetic positron annihilation measurements are shown in Figs. 4(b) and 4(c) as a function of TDD, respectively. The bulk GaN exhibited the smallest S being 0.4401 and the longest [39] $\tau_{PL,eff}$ being 475 ps, and the sample has been identified [31] to have characteristic S for the annihilation of positrons from the defect-free (V_{Ga}-free) *bulk* state (S_{free}). As shown, S of the Si-doped GaN increased with increasing electron density n [Fig. 4(d)], although the data points were limited [31]. The increase in S is explained by the decrease in formation energy of V_{Ga} due to the upward shift of Fermi level (Fermi level effect) [27,29].

It can be seen from Fig. 4(b) that S seems to increase with increasing TDD, though several exceptions existed. This may have two reasons; one is the creation of V_{Ga} around the TDs due to the strain clusters. The other is that TDs act as negatively charged acceptor-type defects like V_{Ga}. Wright and co-workers

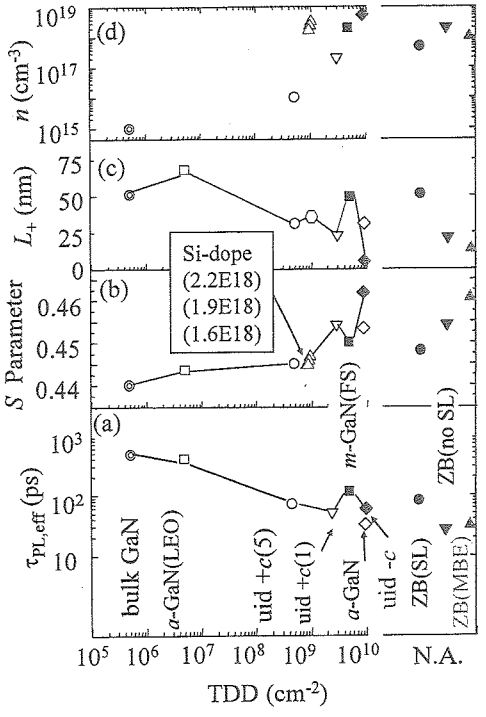

Fig. 4. (a) Effective PL lifetime ($\tau_{PL,eff}$) of the room temperature NBE PL decay, (b) Doppler broadening S parameter of the annihilating γ-rays of positron-electron pairs, (c) positron diffusion length L_d, and (d) electron density n in GaN samples as a function of TDD having edge component. Solid lines are guide to the eye. The horizontal label N. A. for ZB samples means "not analyzed", since the edge dislocations and SFs in ZB GaN are not identical to TDs in wurtzite materials. Samples plotted by closed symbols were unintentionally doped with O. The same symbols are used in Figs. 5 and 6 (after Ref. [35]).

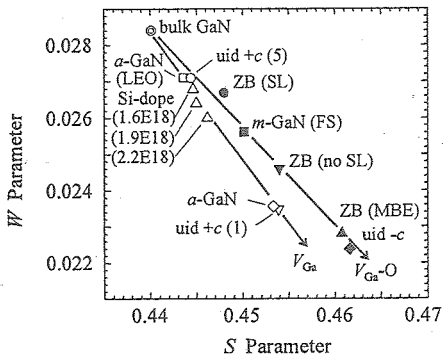

Fig. 5. The *S*-*W* relationship for the GaN samples. Two solid lines with arrows represent the annihilation modes of positrons at (i) defect-free and V_{Ga} (the line denoted by "V_{Ga}") and (ii) defect-free and V_{Ga}-O complexes ("V_{Ga}-O" line) (after Ref. [35]).

[29,30] have calculated the formation energies of point defects in the vicinity of TDs, and concluded that the TD core structure would change depending on the Fermi level and growth stoichiometry, so that the V_{Ga} formation energy became quite high under Ga-rich conditions for *n*-type GaN growth. Therefore, the defect species should be identified before comparing *S* or L_+ and $\tau_{PL,eff}$.

Fig. 5 shows the relationship between *S* and *W*. The (*S*, *W*) plots of the samples represented by open symbols align on the straight line [28,31] denoted by "V_{Ga}". According to Saarinen *et al.* [28] and Uedono *et al.* [31], V_{Ga} is the major point defect that can be detected by positrons, and the line is considered to stay on the tie-line between the annihilation mode of positrons in defect-free state (S_{free}, W_{free}) and that in trapped state for V_{Ga} (S_{VGa}, W_{VGa}) [31]. On the other hand, the (*S*, *W*) plots of the samples represented by closed symbols and bulk GaN align on another straight line denoted by "V_{Ga}-O", which has been assigned to the line connecting (S_{free}, W_{free}) and trapped state for V_{Ga}-O complexes ($S_{VGa\text{-}O}$, $W_{VGa\text{-}O}$) [31]. Indeed, low temperature growth of ZB GaN and N-polar growth of (000-1) GaN introduced O in the epilayers [31,42], and the use of thermally unstable $LiAlO_2$ substrate may cause O diffusion from the substrate [49]. These samples exhibited a relatively strong yellow luminescence (YL) band (orange for ZB ones [42]), whose origin has been reported to be V_{Ga}-O [27,50].

As discussed for Figs. 4(b) and 4(c), the relation between *S* and TDD and that between L_+ and TDD exhibited remarkable exceptions. Hence relations between $\tau_{NR,eff}$ derived from η_{int} and $\tau_{PL,eff}$ using Eqs. 2 and 3 for the NBE PL peak and *S* ($\tau_{NR,eff}$-*S* relation) and between $\tau_{NR,eff}$ and L_+ ($\tau_{NR,eff}$-L_+ relation) in GaN are presented in Figs. 6(a) and 6(b), respectively [11,12,35]. In Fig. 6(a), the S_{free} value of GaN (0.4401) [31] is indicated by the arrow on the upper horizontal axis. As shown by the thick lines in Figs. 6(a) and 6(b), $\tau_{NR,eff}$ increased with the decrease in *S* (reduction in the density of negatively charged defects related to V_{Ga}) and with the increase in L_+ (reduction in gross density of positively-charged, negatively-charged, and neutral point defects). Although the data are not shown, PL intensity naturally increased with increasing $\tau_{NR,eff}$, because $\tau_{R,eff}$ is basically constant in all GaN films. Because $\tau_{NR,eff}$ does not have a perfect correlation with TDD or growth orientations, the dominant parameter that limits $\tau_{NR,eff}$ and thereby η_{int} at 300 K is considered to be the gross concentration of point defects, which are incorporated with V_{Ga} and may be localized around TDs. Certain defect complexes involving V_{Ga} (V_{Ga}-*X*) are the

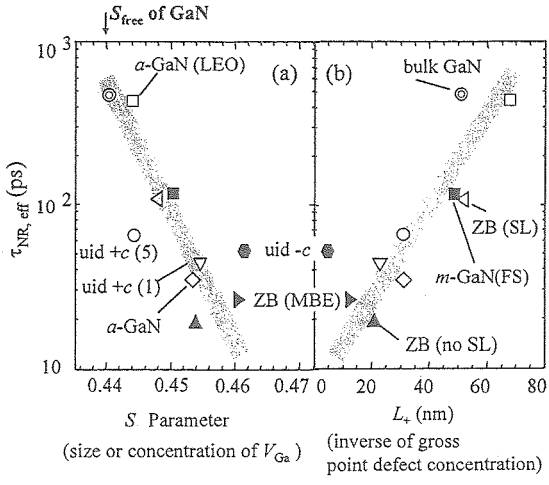

Fig. 6. (a) $\tau_{NR,eff}$-*S* and (b) $\tau_{NR,eff}$-L_+ relations for the NBE PL peak at 300 K in 3D GaN samples having a variety of TDD, orientations, and *n*. The S_{free} value of GaN (0.4401 [31]) is indicated by the arrow on the upper horizontal axis in (a) (after Refs. [11,12,35]).

most probable unique identity of NRCs in GaN [11,12,35]. Here we should mention that TRPL measurements were carried out by monitoring the NBE PL peak, and therefore $\tau_{NR,eff}$ includes both the real $\tau_{NR,eff}$ and the carrier relaxation time to deep levels such as V_{Ga} or V_{Ga}-O complexes. Apparently, they are known as radiative defects, which are the origin of YL band [27,28], but they surely reduce the experimental $\tau_{PL,eff}$. However, there exist other V_{Ga}-related NRCs stated above, since $\tau_{NR,eff}$ of the samples that do not exhibit YL band also obeys the tendency shown in Fig. 6. Because $\tau_{NR,eff}$-S and $\tau_{NR,eff}$-L_+ relations can be approximated by the straight lines for a variety of GaN samples, the lines in Fig. 6 can be treated as *'universal'* scaling lines for GaN, regardless of crystal orientation or symmetry.

AlN study. Recently, a 210 nm electroluminescence (EL) was demonstrated from an AlN *p-i-n* homojunction LED at room temperature [51]. However, its external quantum efficiency (η_{ext}) was extremely low (10^{-6} %). One of the reasons for this is the presence of high-density NRCs. Indeed, AlN suffers from difficulties in growing high quality crystals due to the high melting temperature (~3487 K) [52] and the absence of large-area lattice-matched substrates: the TDD in AlN epitaxial films grown by MOVPE on (0001) Al_2O_3 substrates is generally 10^{10} - 10^{11} cm^{-2} [53]. In addition, AlN epilayers often exhibit characteristic deep emission bands in the energy range between 3 and 5 eV [54-57]. They are invoked to be similar to the YL band in GaN, and to be donor-acceptor pair (DAP) recombinations associated with Al vacancies (V_{Al}) [55,56] and/or defect complexes composed of V_{Al} and oxygen (V_{Al}-O) [54,56,57], although direct proof for the presence of V_{Al} and correlation between the deep band intensity and V_{Al} concentration have not been given yet. Because V_{Ga} in GaN have been shown [35] to form NRCs in a form of V_{Ga}-X complexes, where X is unknown, impacts of V_{Al} incorporation on the emission properties and the dependence of the V_{Al} concentration on the growth parameters must be elucidated.

In this section, results of low-temperature cathodoluminescence (CL) and monoenergetic positron annihilation measurements on AlN epilayers described in the **Samples** section above are shown to correlate the relative intensities of the deep CL bands and concentrations of O and V_{Al}.

A series of CL spectra of the AlN epilayers [44] normalized to the NBE peak intensity at 11 K are shown in Fig. 7. CL was excited with an electron beam operated at 3.5 kV with the emission current density of 1.5 $\times 10^{-2}$ A/cm^2 at sample. The emission was dispersed by a 67-cm-focal length grating monochromator, and phase-sensitive detection synchronized to the beam blanking was carried out using a GaAs:Cs photomultiplier and a solar-blind detector. All the samples exhibited an NBE excitonic emission peak around 6 eV, of which details are discussed later. The samples grown under low V/III ratio or low T_g, both of which correspond to an insufficient nitrogen supply, exhibited additional distinct deep emission bands at 4.6, 3.8, and 3.1 eV. A spectral broadening of the NBE peak was also found for the sample grown under the lowest V/III ratio (60). The relative intensities of these bands over the NBE emission, $I_{4.6eV}$, $I_{3.8eV}$, and $I_{3.1eV}$, respectively, showed an essential decrease with the increase in V/III ratio and T_g, as shown in Fig. 8(a).

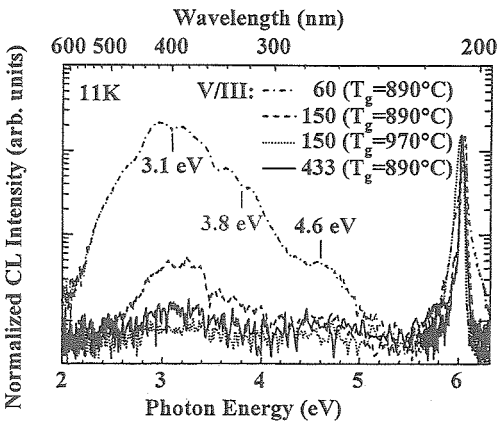

Fig. 7. Normalized CL spectra measured at 11 K of AlN epilayers grown under various supply ratios of NH_3 to Al (V/III ratios) and T_g. The epilayers were grown on (0001) GaN / Al_2O_3 epitaxial templates using an AlN interlayer (IL-AlN) deposited at low temperature (after Ref. [44]).

These emission bands have been invoked as DAP recombinations associated with V_{Al} [57] and/or V_{Al}-O complexes [55-57]. For example, a broad luminescence band at

4~4.5eV in AlN crystals with high O concentrations ($1\sim10\times10^{19}$ cm^{-3}) has been assigned [56] to a DAP emission involving V_{Al}^{3-} - $3O_N^{+}$ complexes. Theoretical calculations have predicted the presence of such defects in AlN [58,59]. Luminescence bands around 3.5 and 4 eV have been assigned [55] to DAP recombinations involving a shallow donor and a deep acceptor, the latter being attributed to V_{Al}^{3-} and V_{Al}-complexes^{2-}. On the other hand, the emissions at 4.6, 3.8, and 3.1 eV have been assigned to originate from V_{Al}, Si-related DX center, and O-related DX center, respectively [57].

These previous assignments are qualitatively consistent with the present results. Since the variation of $I_{4.6eV}$ with V/III ratio and T_g resembles that of S parameter (relative concentration of V_{Al} and/or V_{Al}-complexes), as shown in Figs. 8(a) and 8(b), the band at 4.6 eV is assigned to originate from V_{Al}. On the other hand, because $I_{3.1eV}$ and $I_{3.8eV}$ showed stronger variations with the changes in V/III and T_g, they would have another component in addition to V_{Al}. As their relative intensities greatly increased with the decrease in V/III ratio and T_g, O is one of the probable elements: the increase in V/III ratio (increase in BEP of NH_3) would reduce O incorporation through the competitive incorporation into the group-V sublattice, and high T_g would also reduce the incorporation of volatile O atoms.

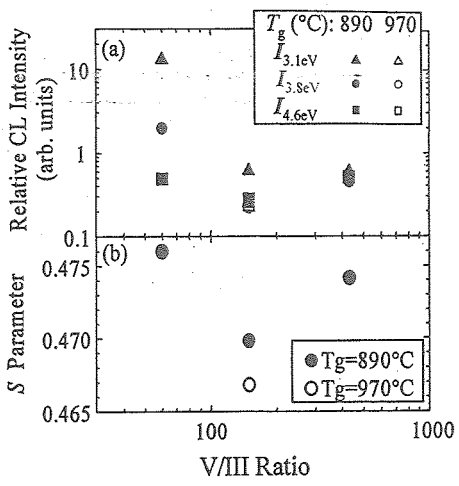

Fig. 8. (a) Intensity ratios of the deep CL bands at 4.6, 3.8, and 3.1 eV to the NBE emission at 11 K of AlN epilayers as functions of V/III ratio and T_g. (b) Doppler broadening S parameter, which is a measure of the concentration (or size) of V_{Al}, of the AlN epilayers as functions of V/III ratio and T_g (after Ref. [44]).

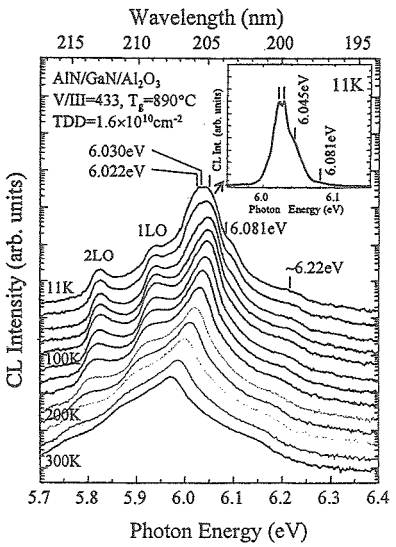

Fig. 9. High resolution NBE CL spectra of the AlN epilayer as a function of temperature. The inset shows the NBE spectrum at 11 K (linear y-axis) (after Ref. [44]).

It should be noted that the S parameter of the samples grown with V/III = 150 was the smallest, presumably because the surface stoichiometry was maintained: the increase in V/III may turn it into N-rich growth condition and the decrease in V/III may give rise to donor (O) incorporation, which results in the formation of V_{Al} due to the Fermi-level effect [59]. As TDD in the present samples exhibited positive correlations with $I_{3.1eV}$, $I_{3.8eV}$ and S, TDs may incorporate O and V_{Al}. According to Nam *et al.* [55], the electron energy of the V_{Al}^{3-} level is approximately 0.5 eV higher than the $(V_{Al}$-complex$)^{2-}$ level. Therefore, the bands at 3.8 eV and 3.1 eV might be assigned as being due to the emissions associated with $(V_{Al}$-complex$)^{2-}$-O and V_{Al}^{3-}-O, respectively. Judging from the large FWHM of the bands, they seem to form DX centers.

As a result of the decrease in V_{Al} (and O) concentration, AlN epilayers exhibiting negligible deep level emissions were obtained, as shown in Fig. 7. Since defect complexes composed of cation vacancies (V_{III}-X) act as NRCs in GaN and AlGaN [11,12,35], V_{Al}-X might act as NRCs in AlN. Indeed, the NBE emission intensity at room temperature of the samples

grown with V/III = 150 (T_g = 970°C and 870°C) was greatly improved. High-resolution CL spectra of the sample grown with V/III = 433 and T_g = 890°C are shown in Fig. 9 as a function of measurement temperature. Inset shows the NBE spectrum at 11 K (linear y-axis). As shown, the spectrum at 11 K exhibited two peaks at 6.022 and 6.030 eV, two shoulders at 6.045 and 6.081 eV, and a broad peak at around 6.22 eV. Because the peaks at 6.022 and 6.030 eV showed faster thermal quenching than the shoulder at 6.045 eV, they are assigned to the recombinations of excitons bound to neutral donors (D^0, X). Silveira *et al.* [60] have determined the energies of free excitons as 6.029, 6.243, and 6.268 eV for A-, B-, and C-excitons, respectively, from low temperature optical reflectance spectrum of AlN single crystals. According to the first-principles calculation of the band structure, Li *et al.* [61] have determined the energy separations between A- and B-excitons (213 meV) and B- and C-excitons (13 meV). Since the emissions at 6.045 eV and 6.22 eV became dominant except for LO phonon replicas as temperature was increased, they are assigned to the recombinations of free A-excitons and free B- and C-excitons, respectively. A slight blueshift of the A-exciton peak from 6.029 eV [60] to 6.045 eV is due to the compressive stress in our AlN / GaN / Al_2O_3 epilayer [62], which was confirmed by x-ray diffraction measurements. The shoulder at 6.081 eV is assigned to the recombination of the first-excited state of an A-exciton [63]. From the energy separation between the ground and first excited states, the binding energy of A-exciton is determined to be 48 meV. We note that an emission peak originating from the first excited state of an A-exciton was observed from the film having TDD as high as 1.6×10^{10} cm^{-2}, because the A-exciton Bohr radius in AlN is as small as 1.9 nm.

AlGaN alloy films. In order to expand the operation wavelength of LEDs and LDs into UV regions, research efforts are being made for the growth of device quality $Al_xGa_{1-x}N$ alloys. However, η of AlGaN alloys is still worse than that of InGaN alloys, and the threshold power density to observe the stimulated emission has been reported to increase with increasing x [64]. Therefore, it is important to investigate what dominates the low η. While a number of papers have been published on steady-state optical properties of AlGaN epitaxial films, few reported results have been available on the emission dynamics in AlGaN films [47,65,66]. In addition, the role of point defects on the nonradiative processes and the formation of deep levels has not been disclosed yet. In this section, results of steady-state and time-resolved PL of nearly strain-free $Al_xGa_{1-x}N$ alloys were compared with the results of positron annihilation measurements to elucidate the roles of point defects.

PL or CL spectra of 3D $Al_xGa_{1-x}N$ alloy films 300 K are summarized in Fig. 10. The TDD of the samples was of the order of 10^{10} cm^{-2}. As shown, the samples exhibited an NBE emission and a characteristic deep emission band, and the intensity of the latter increased with x up to 0.75. Values of η_{int} at 300 K for the NBE emission of the films are plotted as a function of AlN molar fraction x in Fig. 11(a). For comparison, corresponding values for 3D GaN films with a variety of TDDs, growth polar directions, orientations, and background electron concentrations are represented by a rectangle on the vertical axis. The values of $\tau_{NR,eff}$ and $\tau_{R,eff}$ for the NBE emission at 293 K obtained from η_{int} and $\tau_{PL,eff}$ using Eqs. 2 and 3 are plotted in Figs. 11(b) and 11(c), respectively. It is found from Fig. 11 that $\tau_{NR,eff}$ stays 'nearly' constant but $\tau_{R,eff}$ increases (and hence η_{int} decreases) with an increase in x. This result suggests the presence of certain bound states [47] or carrier reservoirs that act as trapping state and/or a decrease in oscillator strength with increasing x [67].

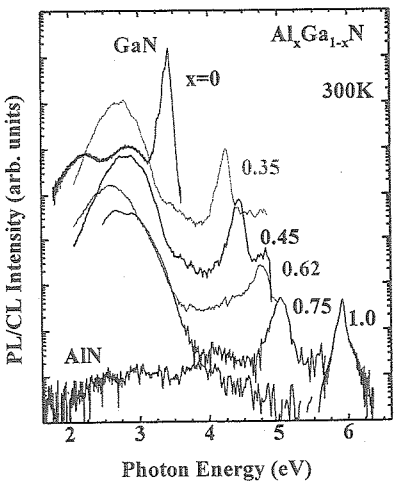

Fig. 10. PL or CL spectra of nearly strain-free $Al_xGa_{1-x}N$ films measured at 300 K. They were grown on (0001) Al_2O_3 substrates using an $Al_{0.63}Ga_{0.37}N$ NL layer (after Ref. [47]).

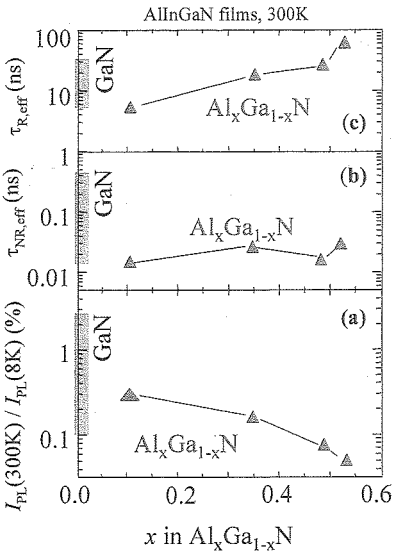

Fig. 11. Values of (a) spectrally-integrated PL intensity of the NBE emission peak at 300 K divided by that at 8 K [I_{PL}(300K) / I_{PL}(8K)], which is representative of η_{int} [36], (b) $\tau_{NR,eff}$, and (c) $\tau_{R,eff}$ for the NBE emission of 3D $Al_xGa_{1-x}N$ films as a function of x. For comparison, corresponding values for 3D GaN films with a variety of TDDs, growth polar directions, orientations, and electron concentrations are shown by rectangles on the vertical axis (after Refs. [11,12]).

defective. It should be noted that the formation energy of V_{Al} in AlN [33] (and in AlGaN) is lower that that of V_{Ga} in GaN [32,34]. Therefore, the nonradiative recombination rate through V_{Al}-X defects in $Al_xGa_{1-x}N$ is considered to increase with x.

The spectrally-integrated intensities of the deep emission bands over that of the NBE emission, $\Sigma I_{deep}/\Sigma I_{NBE}$ (see Fig. 10) in the $Al_xGa_{1-x}N$ films are shown as a function of x in Fig. 13(a). As shown, $\Sigma I_{deep}/\Sigma I_{NBE}$ increased with x and showed a maximum around x=0.75. On the analogy of GaN and AlN, influences of V_{III} were investigated using monoenergetic positron annihilation measurements: values of S and L_+ are plotted in Figs. 13(b) and 13(c) as a function of x, respectively. For

As is the case with GaN (Fig. 6), $\tau_{NR,eff}$-S and $\tau_{NR,eff}$-L_+ relations for the $Al_xGa_{1-x}N$ alloy films (x=0.35, 0.45, 0.52) at 300 K are plotted in Fig. 12(a) and 12(b), respectively, in which *the universal scaling lines* drawn for GaN [11,12,35] are represented by the grey lines. In Fig. 12(a), the S_{free} value of GaN (0.4401) [31] is indicated by the arrow on the upper horizontal axis. The S_{free} value of AlN is yet unknown. However, it must be smaller than 0.4614 [47]. Dannefaer *et al.* [68] have found a linear relation between the S parameter and r_s in most of III-V semiconductors, where r_s is the radius of free-electron gas and

$$\frac{4\pi}{3} r_s^3 = n_{val}^{-1}, \tag{7}$$

where n_{val} is the density of valence electrons as based on all available volume. Since the lattice parameter of AlN is close to that of GaN and the number of valence electrons is exactly the same in both compounds, the r_s value of AlN (0.86) is very close to that of GaN (0.88). Therefore, defect-free AlN is considered to have a characteristic S value similar to that of bulk defect-free GaN. Since the S_{free} reflects the chemical composition of the alloy, the S parameter of the defect-free $Al_xGa_{1-x}N$ lattice is also considered to be approximately the same as the value in GaN (0.44). The result that the data for $Al_xGa_{1-x}N$ aligned on the bottom portions of the $\tau_{NR,eff}$-S and $\tau_{NR,eff}$-L_+ lines of GaN indicates that NRCs in AlGaN and GaN films have similar origins. From the large S, short L_+, and short $\tau_{NR,eff}$ values, AlGaN films having TDD of the order of 10^{10} cm^{-2} are confirmed to be

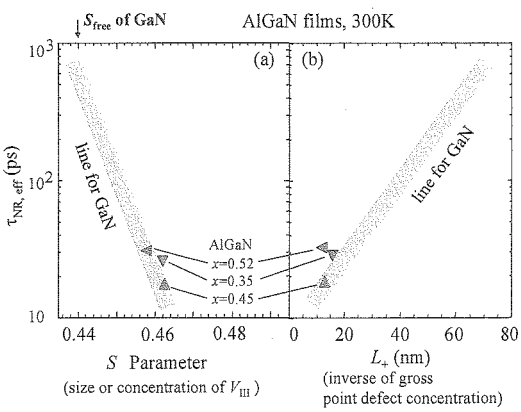

Fig. 12. (a) $\tau_{NR,eff}$-S and (b) $\tau_{NR,eff}$-L_+ relations for the NBE PL peak at 300 K in 3D $Al_xGa_{1-x}N$ films. The *universal lines* drawn for a variety of GaN samples are represented by thick grey lines. The S_{free} value of GaN (0.4401 [31]) is indicated by the arrow on the upper horizontal axis in (a) (after Refs. [11,12,35]).

comparison, corresponding values for the GaN films containing different V_{Ga} concentrations are plotted on the vertical axis (x=0). The values S≅0.44 and L_+=51 nm denoted by "undoped (LEO)" correspond to those of the annihilation of positrons in nearly V_{Ga}-free GaN background [31]. As described in the previous section, S_{free} of AlN and AlGaN may be similar to that of GaN being 0.44. Therefore, the increase in S in AlGaN alloys shown in Fig. 13(b) indicates the increase in size/density of V_{III} defects. Obviously, the S value has the maximum around x=0.7, which may reflect the increase in the mixing entropy in AlGaN alloys. Since the variation of $\Sigma I_{deep}/\Sigma I_{NBE}$ with x resembles that of S, the bands are assigned to originate from V_{III}. Because the formation energy of V_{Al} in AlN is lower than that of V_{Ga} in GaN [27,29,34,59] and the peak energies of the deep bands in AlGaN are close to that of the 3.1 eV band in AlN, as recognized from Figs. 7 and 10, the deep bands may be mostly related to V_{Al}-O complexes rather than V_{Ga} ones.

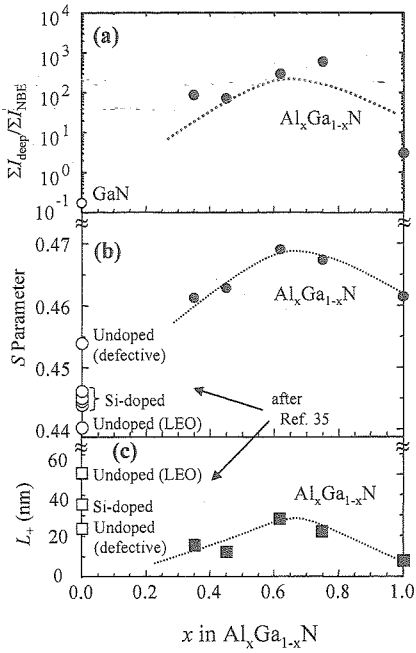

Fig. 13. (a) Spectrally-integrated intensities of the deep emission bands over that of the NBE emission, $\Sigma I_{deep}/\Sigma I_{NBE}$, (b) S parameter, and (c) L_+ of $Al_xGa_{1-x}N$ films (closed characters) as a function of x. Corresponding values for the GaN films containing different V_{Ga} concentrations are plotted on the vertical axis (x=0) for comparison (after Ref.s. [31,47]).

It has been proposed that O forms a DX center, which is a complex defect level composed of a certain donor and other components, in $Al_xGa_{1-x}N$ alloys [69-71] especially for x>0.3 [70]. Since O is the most probable impurity during the MOVPE growth of AlGaN films at relatively low T_g, formation of DX centers is probable, which may elongate $\tau_{R,eff}$ of the NBE emission. Indeed, the O concentration in the $Al_{0.63}Ga_{0.37}N$ was quantified by secondary-ion mass spectroscopy to be 1×10^{17} cm^{-3} [47]. It is also interesting to note from Figs. 13(b) and 13(c) that $Al_xGa_{1-x}N$ films having x nearly 0.7 exhibited the maximum S and L_+. The result is opposite to the case for GaN, where the increase of S accompanied the decrease in L_+, as recognized from Figs. 4(b) and 4(c). The latter result is reasonable, since the increase in S means the increase in V_{Ga} concentration and the decrease of L_+ means the increase in the gross concentration of V_{Ga} and positron scattering centers. However, the increase in S induced the increase in L_+ in the present $Al_xGa_{1-x}N$. The result indicates that the V_{III} concentration increases with x up to 0.7, but the total concentration of positron scattering centers decreases simultaneously. This can be explained by an effective neutralization of positively-charged positron scattering centers (interstitials and ionized donors) by the introduction of V_{III}. Then, the formation of V_{III}-O_N, V_{III}-Si_N, or V_{III}-X_i may be enhanced with increasing x. Since the change in $\tau_{R,eff}$ with x exhibited similar trend as that of V_{III} concentration, these V_{III}-related complexes are possible origins of the carrier reservoir acting as trapping states.

Summary

The principal roles of cation vacancies on the luminescent properties of GaN, AlN, and AlGaN alloys were investigated using TRPL and positron annihilation measurements. The origin of NRCs in GaN is proposed to be certain complexes involving V_{Ga}, such as V_{Ga}-X, from the *universal scaling lines* established in τ_{NR}-S and τ_{NR}-L_+ relations for a variety of GaN films. Similar relations were found for $Al_xGa_{1-x}N$ alloy films: *i. e.* τ_{NR} at room temperature increased with the decrease in the concentration

of cation vacancies (V_{III}) and with the decrease in gross concentration of point defects. In addition to the nonradiative process, the V_{III} concentration was found to correlate with the relative intensity of characteristic deep emission bands in (Al,Ga)N. For example, from the relations between S and W parameters for nearly oxygen-free and oxygen-containing GaN films, YL in GaN is assigned to originate from V_{Ga}-O complexes. Similarly, the deep emission bands at 3.1 and 3.8 eV in AlN films are assigned to originate from V_{Al}-O as well as V_{Al}-shallow donor complexes. A similar conclusion is also drawn for $Al_xGa_{1-x}N$ alloy films. From the relations among the relative intensity, S parameter, and growth conditions, the deep emission band at 4.5 eV in AlN is assigned to originate from V_{Al}. We note that V_{Al} concentration could be decreased by adjusting the V/III ratio and T_g, indicating that stoichiometry maintenance is one of the potential protocols to reduce the vacancy-defect concentration in (Al,Ga)N.

Acknowledgments

The research work described here were supported in parts by Exploratory Research for Advanced Technology, Japan Science and Technology Agency, DARPA, AOARD-AFOSR, CANTech, IMRAM, Tohoku University, the 21st Century COE program "Promotion of Creative Interdisciplinary Materials Science for Novel Functions", the Global COE program "Materials Integration", and a Grant-in-Aid for Scientific Research in Priority Areas No. 18069001 under MEXT, Japan.

References

[1] S. Nakamura and G. Fasol: *The Blue Laser Diode* (Springer, Berlin, 1997).

[2] I. Akasaki and H. Amano: Japan J. Appl. Phys. **36**, 5393 (1997).

[3] F.A. Ponce and D. Bour: Nature **386**, 351 (1997).

[4] S. Chichibu, T. Azuhata, T. Sota and S. Nakamura: Appl. Phys. Lett. **69**, 4188 (1996).

[5] C. Kisielowski, Z. Liliental-Weber and S. Nakamura: Japan. J. Appl. Phys. **36**, 6932 (1997).

[6] Y. Narukawa, Y. Kawakami, M. Funato, Sz. Fujita, Sg. Fujita and S. Nakamura: Appl. Phys. Lett. **70**, 981 (1997).

[7] S. Chichibu, K. Wada and S. Nakamura: Appl. Phys. Lett. **71**, 2346 (1997).

[8] L. Bellaiche, T. Mattila, L.W. Wang, S.-H. Wei and A. Zunger: Appl. Phys. Lett. **74**, 1842 (1999).

[9] P.R.C. Kent and A. Zunger: Appl. Phys. Lett. **79**, 1977 (2001).

[10] L.-W. Wang: Phys Rev. B **63**, 245107 (2001).

[11] S.F. Chichibu, A.Uedono, T. Onuma, B.A. Haskell, A. Chakraborty, T. Koyama, P.T. Fini, S. Keller, S.P. DenBaars, J.S. Speck, U.K. Mishra, S. Nakamura, S. Yamaguchi, S. Kamiyama, H. Amano, I. Akasaki, J. Han and T. Sota: Nature Materials **5**, 810 (2006).

[12] S.F. Chichibu, A.Uedono, T. Onuma, B.A. Haskell, A. Chakraborty, T. Koyama, P.T. Fini, S. Keller, S.P. DenBaars, J.S. Speck, U.K. Mishra, S. Nakamura, S. Yamaguchi, S. Kamiyama, H. Amano, I. Akasaki, J. Han and T. Sota: Philos. Mag. **87**, 2019 (2007).

[13] X. Wu, C.R. Elsass, A.C. Abare, M.P. Mack, S. Keller, P. Petroff, S.P. DenBaars, J.S. Speck and S.J. Rosner: Appl. Phys. Lett. **72**, 692 (1998).

[14] S.F. Chichibu, A.C. Abare, M.P. Mack, M. Minsky, T. Deguchi, D. Cohen, P. Kozodoy, S.B. Fleischer, S. Keller, J.S. Speck, J.E. Bowers, E. Hu, U.K. Mishra, L.A. Coldren, S.P. DenBaars, K. Wada, T. Sota and S. Nakamura: Mat. Sci. Eng. B **59**, 298 (1999).

[15] K.P. O'Donnell, R.W. Martin and P.G. Middleton: Phys. Rev. Lett. **82**, 237 (1999).

[16] A. Hangleiter, J.S. Im, J. Off and F. Scholz: Phys. Stat. Solidi (b) **216**, 427 (1999).

[17] C. Wetzel, T. Takeuchi, H. Amano and I. Akasaki: Japan. J. Appl. Phys. **38**, L163 (1999).

[18] S.F. Chichibu, T. Sota, K. Wada, O. Brandt, K.H. Ploog, S.P. DenBaars and S. Nakamura: Phys. Stat. Solidi (a) **183**, 91 (2001).

[19] S. Pereira, M.R. Correia, E. Pereira, C. Trager-Cowan, F. Sweeney, K.P. O'Donnell, E. Alves, N. Franco and A.D. Sequeira: Appl. Phys. Lett. **81**, 1207 (2002).

[20] T.M. Smeeton, M.J. Kappers, J.S. Barnard, M.E. Vickers and C.J. Humphreys: Appl. Phys. Lett. **83**, 4519 (2003).

[21] S.F. Chichibu, T. Onuma, T. Aoyama, K. Nakajima, P. Ahmet, T. Chikyow, T. Sota, S.P. DenBaars, S. Nakamura, T. Kitamura, Y. Ishida and H. Okumura: J. Vac. Sci. Technol. B **21**, 1856 (2003).

[22] F.A. Ponce, S. Srinivasan, A. Bell, L. Geng, R. Liu, M. Stevens, J. Cai, H. Omiya, H. Marui and S. Tanaka: Phys. Stat. Solidi (b) **240**, 273 (2003).

[23] A. Morel, P. Lefebvre, S. Kalliakos, T. Taliercio, T. Bretagnon and B. Gil: Phys. Rev. B **68**, 045331 (2003).

[24] W. Walukiewicz, S.X. Li, J. Wu, K.M. Yu, J.W. Ager III, E.E. Haller, H. Lu and W.J. Schaff: J. Cryst. Growth **269**, 119 (2004).

[25] A. Hangleiter, F. Hitzel, C. Netzel, D. Fuhrmann, U. Rossow, G. Ade and P. Hinze: Phys. Rev. Lett. **95**, 127402 (2005).

[26] T. Sugahara, H. Sato, M. Hao, Y. Naoi, S. Kurai, S. Tottori, K. Yamashita, K. Nishino, L. T. Romano and S. Sakai: Jpn. J. Appl. Phys. **37**, L398 (1998).

[27] J. Neugebauer and C.G. Van de Walle: Phys. Rev. B **50**, 8067 (1994).

[28] K. Saarinen, T. Laine, S. Kuisma, J. Nissilä, P. Hautojärvi, L. Dobrzynski, J.M. Baranowski, K. Pakula, R. Stepniewski, M. Wojdak, A. Wysmolek, T. Suski, M. Leszczynski, I. Grzegory and S. Porowski: Phys. Rev. Lett. **79**, 3030 (1997).

[29] A. F. Wright and U. Grossner: Appl. Phys. Lett. **73**, 2751 (1998).

[30] K. Leung, A. F. Wright and E. B. Stechel: Appl. Phys. Lett. **74**, 2495 (1999).

[31] A. Uedono, S.F. Chichibu, Z.Q. Chen, M. Sumiya, R. Suzuki, T. Ohdaira, T. Mikado, T. Mukai and S. Nakamura: J. Appl. Phys. **90**, 181 (2001).

[32] A.F. Wright: J. Appl. Phys. **90**, 1164 (2001).

[33] C. Stampfl and C.G. Van de Walle: Phys. Rev. B **65**, 155212 (2002).

[34] C.G. Van de Walle and J. Neugebauer: J. Appl. Phys. **95**, 3851 (2004).

[35] S.F. Chichibu, A. Uedono, T. Onuma, T. Sota, B.A. Haskell, S.P. DenBaars, J.S. Speck and S. Nakamura: Appl. Phys. Lett. **86**, 021914 (2005).

[36] Y. Narukawa, Y. Kawakami, Sg. Fujita and S. Nakamura: Phys. Rev. B **59**, 10283 (1999).

[37] R. Krause-Rehberg and H.S. Leipner, in: *Positron Annihilation in Semiconductors*, Solid-State Sciences 127, Springer, Berlin (1999).

[38] P.G. Coleman, in: *Positron Beams and Their Application*, World Scientific, Singapore (2000).

[39] S.F. Chichibu, H. Marchand, M.S. Minsky, S. Keller, P.T. Fini, J.P. Ibbetson, S.B. Fleischer, J.S. Speck, J.E. Bowers, E. Hu, U.K. Mishra, S.P. DenBaars, T. Deguchi, T. Sota and S. Nakamura: Appl. Phys. Lett. **74**, 1460 (1999).

[40] S. Chichibu, T. Azuhata, T. Sota and S. Nakamura: J. Appl. Phys. **79**, 2784 (1996).

[41] S.F. Chichibu, A. Setoguchi, A. Uedono, K. Yoshimura and M. Sumiya: Appl. Phys. Lett. **78**, 28 (2001).

[42] S.F. Chichibu, M. Sugiyama, T. Nozaka, T. Suzuki, T. Onuma, K. Nakajima, T. Aoyama, M. Sumiya, T. Chikyow and A. Uedono: J. Cryst. Growth **272**, 481 (2004).

[43] B.A. Haskell, F. Wu, M.D. Craven, S. Matsuda, P.T. Fini, T. Fujii, K. Fujito, S.P. DenBaars, J.S. Speck and S. Nakamura: Appl. Phys. Lett. **83**, 644 (2003).

[44] T. Koyama, M. Sugawara, T. Hoshi, A. Uedono, J.F. Kaeding, R. Sharma, S. Nakamura and S.F. Chichibu: Appl. Phys. Lett. **90**, 241914 (2007).

[45] S. Kamiyama, M. Iwaya, N. Hayashi, T. Takeuchi, H. Amano, I. Akasaki, S. Watanabe, Y. Kaneko and N. Yamada: J. Cryst. Growth **223**, 83 (2001).

[46] C. G. Dunn and E. F. Koch: Acta Metall. **5**, 548 (1957).

[47] T. Onuma, S.F. Chichibu, A. Uedono, T. Sota, P. Cantu, T.M. Katona, J.F. Keading, S. Keller, U.K. Mishra, S. Nakamura and S.P. DenBaars: J. Appl. Phys. **95**, 2495 (2004).

[48] A. Van Veen, H. Schut, M. Clement, J.M.M. de Nijs, A. Kruseman and M.R. Ijpma: Appl. Surf. Sci. **85**, 216 (1995).

[49] P. Waltereit, O. Brandt, A. Trampert, H.T. Grahn, J. Menniger, M. Ramsteiner, M. Reiche and K. H. Ploog: Nature **406**, 865 (2000).

[50] J. Neugebauer and C.G. Van de Walle: Appl. Phys. Lett. **69**, 503 (1996).

[51] Y. Taniyasu, M. Kasu and T. Makimoto: Nature **441**, 325 (2006).

[52] J.A. Van Vechten: Phys. Rev. B **7**, 1479 (1973).

[53] T. Shibata, K. Asai, S. Sumiya, M. Mouri, M. Tanaka, O. Oda, H. Katsukawa, H. Miyake and K. Hiramatsu: Phys. Stat. sol. (c) **0**, 2023 (2003).

[54] G.A. Slack, L.J. Schowalter, D. Morelli and J.A. Freitas Jr.: J. Cryst. Growth **246**, 287 (2002).

[55] K.B. Nam, M.L. Nakarmi, J.Y. Lin and H.X. Jiang: Appl. Phys. Lett. **86**, 222108 (2005).

[56] E. Monroy, J. Zenneck, G. Cherkashinin, O. Ambacher, M. Hermann, M. Stutzmann: and M. Eickhoff: Appl. Phys. Lett. **88**, 071906 (2006).

[57] A. Dadgar, A. Krost, J. Christen, B. Bastek, F. Bertram, A. Krtschil, T. Hempel, J. Bläsing, U. Haboeck and A. Hoffmann: J. Cryst. Growth **297**, 306 (2006).

[58] T. Mattila and R.M. Nieminen: Phys. Rev. B **54**, 16676 (1996).

[59] C. Stampfl and C.G. Van de Walle: Appl. Phys. Lett. **72**, 459 (1998).

[60] E. Silveira, J.A. Freitas, Jr., O.J. Glembocki, G.A. Slack and L.J. Schowalter: Phys. Rev. B **71**, 041201 (2005).

[61] J. Li, K. B. Nam, M.L. Nakarmi, J.Y. Lin, H.X. Jiang, P. Carrier and S.-H. Wei, Appl. Phys. Lett. **83**, 5163 (2003).

[62] H. Ikeda, T. Okamura, K. Matsukawa, T. Sota, M. Sugawara, T. Hoshi, P. Cantu, R. Sharma, J.F. Kaeding, S. Keller, U.K. Mishra, K. Kosaka, K. Asai, S. Sumiya, T. Shibata, M. Tanaka, J.S.

Speck, S.P. DenBaars, S. Nakamura, T. Koyama, T. Onuma, and S.F. Chichibu: J. Appl. Phys. **102**, 123707 (2007).

[63] E. Silveira, J.A. Freitas, Jr., M. Kneissl, D.W. Treat, N.M. Johnson, G.A. Slack and L.J. Schowalter: Appl. Phys. Lett. **84**, 3501 (2004).

[64] T.J. Schmidt, Y.H. Cho, J.J. Song and W. Yang: Appl. Phys. Lett. **74**, 245 (1999).

[65] Y.H. Cho, G.H. Gainer, J.B. Lam, J.J. Song, W. Yang and W. Jhe: Phys. Rev. B **61**, 7203 (2000).

[66] H.S. Kim, R.A. Mair, J. Li, J.Y. Lin, and H.X. Jiang: Appl. Phys. Lett. **76**, 1252 (2000).

[67] S.V. Dudiy and A. Zunger: Appl. Phys. Lett. **84** 1874 (2004).

[68] S. Dannefaer, W. Puff and D. Kerr: Phys. Rev. B **55**, 2182 (1997).

[69] C. Wetzel, T. Suski, J.W. Ager III, E.R. Weber, E.E. Haller, S. Fisher, B. Meyer, R. Molnar and P. Perlin: Phys. Rev. Lett. **78**, 3923 (1997).

[70] M.D. McCluskey, N.M. Johnson, C.G. Van de Walle, D.P. Bour, M. Kneissl and W. Walukiewicz: Phys. Rev. Lett. **80**, 4008 (1998).

[71] C. Skierbiszewski, T. Suski, M. Leszczynski, M. Shin, M. Skowronski, M.D. Bremser and R.F. Davis: Appl. Phys. Lett. **74**, 3833 (1999).